Inorg. Chem. **2007**, *46*, 8625–8637

Probing Lead(II) Bonding Environments in 4-Substituted Pyridine Adducts of $(2,6\text{-}Me_2C_6H_3S)_2Pb$: An X-ray Structural and Solid-State ^{207}Pb NMR Study

Glen G. Briand,*,† Andrew D. Smith,† Gabriele Schatte,‡ Aaron J. Rossini,§ and Robert W. Schurko*,§

Department of Chemistry, Mount Allison University, Sackville, New Brunswick, Canada E4L 1G8, Saskatchewan Structural Sciences Centre, University of Saskatchewan, Saskatoon, Saskatchewan Canada S7N 5C9, and Department of Chemistry & Biochemistry, University of Windsor, Windsor, Ontario, Canada N9B 3P4

Received April 18, 2007

The effect of subtle changes in the σ-electron donor ability of 4-substituted pyridine ligands on the lead(II) coordination environment of $(2,6\text{-}Me_2C_6H_3S)_2Pb$ (**1**) adducts has been examined. The reaction of **1** with a series of 4-substituted pyridines in toluene or dichloromethane results in the formation of 1:1 complexes $[(2,6\text{-}Me_2C_6H_3S)_2Pb(pyCOH)]_2$ (**3**), $[(2,6\text{-}Me_2C_6H_3S)_2Pb(pyOMe)]_2$ (**4**), and $(2,6\text{-}Me_2C_6H_3S)_2Pb(pyNMe_2)$ (**5**) (pyCOH = 4-pyridinecarboxaldehyde; pyOMe = 4-methoxypyridine; $pyNMe_2$ = 4-dimethylaminopyridine), all of which have been structurally characterized by X-ray crystallography. The structures of **3** and **4** are dimeric and have ψ-trigonal bipyramidal S_3N bonding environments, with the 4-substituted pyridine nitrogen and bridging sulfur atoms in axial positions and two thiolate sulfur atoms in equatorial sites. Conversely, compound **5** is monomeric and exhibits a ψ-trigonal pyramidal S_2N bonding environment at lead(II). The observed structures may be rationalized in terms of a simple valence bond model and the σ-electron donor ability of the 4-pyridine ligands as derived from the analysis of proton affinity values. Solid-state ^{207}Pb NMR experiments are applied in combination with density functional theory (DFT) calculations to provide further insight into the nature of bonding in **4**, **5**, and $(2,6\text{-}Me_2C_6H_3S)_2Pb(py)_2$ (**2**). The lead chemical shielding (CS) tensor parameters of **2**, **4**, and **5** reveal some of the largest chemical shielding anisotropies (CSA) observed in lead coordination complexes to date. DFT calculations using the *Amsterdam Density Functional* (*ADF*) program, which take into account relativistic effects using the zeroth-order regular approximation (ZORA), yield lead CS tensor components and orientations. Paramagnetic contributions to the lead CS tensor from individual pairs of occupied and virtual molecular orbitals (MOs) are examined to gain insight into the origin of the large CSA. The CS tensor is primarily influenced by mixing of the occupied MOs localized on the sulfur and lead atoms with virtual MOs largely comprised of lead 6p orbitals.

Introduction

There has been increasing interest in the preparation of nanocrystals of narrow band gap semiconducting materials for use in optoelectronic devices.[1−6] In particular, the production of lead sulfide (PbS) nanocrystals has been extensively studied and has been achieved via a variety of synthetic routes.[7−13] It has recently been shown that lead(II) thiolates represent possible organometallic precursors for the

* To whom correspondence should be addressed. E-mail: gbriand@mta.ca. Tel: (506) 364-2346. Fax: (506) 364-2313 (G.G.B.), E-mail: rschurko@uwindsor.ca. Tel: (519) 253-3000 x3548. Fax: (519) 973-7098 (R.W.S.).
† Mount Allison University.
‡ University of Saskatchewan.
§ University of Windsor.

(1) Chang, T. W. F.; Musikhin, S.; Bakueva, L.; Levina, L.; Hines, M. A.; Cyr, P. W.; Sargent, E. H. *Appl. Phys. Lett.* **2004**, *84*, 4295.
(2) Kim, S.; Fisher, B.; Eisler, H. J.; Bawendi, M. *J. Am. Chem. Soc.* **2003**, *125*, 11466.
(3) McDonald, S. A.; Cyr, P. W.; Levina, L.; Sargent, E. H. *Appl. Phys. Lett.* **2004**, *85*, 2089.
(4) McDonald, S. A.; Konstantatos, G.; Zhang, S. G.; Cyr, P. W.; Klem, E. J. D.; Levina, L.; Sargent, E. H. *Nat. Mater.* **2005**, *4*, 138.
(5) Sargent, E. H. *J. Mod. Opt.* **2004**, *51*, 2797.
(6) Sukhovatkin, V.; Musikhin, S.; Gorelikov, I.; Cauchi, S.; Bakueva, L.; Kumacheva, E.; Sargent, E. H. *Opt. Lett.* **2005**, *30*, 171.
(7) Bakueva, L.; Gorelikov, I.; Musikhin, S.; Zhao, X. S.; Sargent, E. H.; Kumacheva, E. *Adv. Mater.* **2004**, *16*, 926.
(8) Buckner, S. W.; Konold, R. L.; Jelliss, P. A. *Chem. Phys. Lett.* **2004**, *394*, 400.
(9) Fernee, M. J.; Watt, A.; Warner, J.; Heckenberg, N.; Rubinsztein-Dunlop, H. *Nanotechnology* **2004**, *15*, 1328.

10.1021/ic700738w CCC: $37.00
Published on Web 09/15/2007

production of interesting thiolate-capped clusters and nanocrystals.[14−17] As a result of the well-known toxicity of lead(II) complexes, there is also much interest in the synthesis of simple coordination compounds to better understand the binding of lead(II) by the cysteine residues of biomolecules.[18−21]

Although they have been known for a number of decades,[14,15] the inherent insolubility and nonvolatility associated with lead(II) thiolates has resulted in the delayed development of their chemistry. The few structural studies that have been undertaken show that simple lead(II) thiolates $(RS)_2Pb$ (R = C_6H_5, 4-MeC_6H_4, CH_2) possess polymeric structures in the solid state as a result of extensive intermolecular Pb···S interactions.[22−24] The resulting high coordination numbers for lead(II) in these compounds, along with its empty p orbitals and variable stereochemical activity of the valence electron lone pair,[25] suggest a potentially rich coordination chemistry that has remained relatively unexplored.[18,26−28]

In this context, we have recently reported the preparation of the 2,6-substituted arylthiolate $(2,6\text{-}Me_2C_6H_3S)_2Pb$ (**1**), which has an increased solubility in comparison to the alkyl- and unsubstituted arylthiolate [i.e., $(PhS)_2Pb$] analogues.[29] The reaction of **1** with pyridine (py) yielded the 1:2 adduct $(2,6\text{-}Me_2C_6H_3S)_2Pb(py)_2$ (**2**), which is monomeric and exhibits no intermolecular Pb···S contacts. Further, bridging Lewis-base ligands, 4,4′-bipyridyl (bipy) and pyrazine (pyr), afforded the 1:1 coordination polymers $[(2,6\text{-}Me_2C_6H_3S)_2Pb(L)]_\infty$ (L = bipy, pyr). Interestingly, all of the complexes show ψ-trigonal bipyramidal S_2N_2 coordination geometries,

Chart 1. Schematic Drawings of Lead Thiolate Structures, Including $(2,6\text{-}Me_2C_6H_3S)_2Pb(py)_2$ (**2**), $[(2,6\text{-}Me_2C_6H_3S)_2Pb(pyCOH)]_2$ (**3**), $[(2,6\text{-}Me_2C_6H_3S)_2Pb(pyOMe)]_2$ (**4**), and $(2,6\text{-}Me_2C_6H_3S)_2Pb(pyNMe_2)$ (**5**) (py = Pyridine; pyCOH = 4-Pyridinecarboxaldehyde; pyOMe = 4-Methoxypyridine; $pyNMe_2$ = 4-Dimethylaminopyridine)

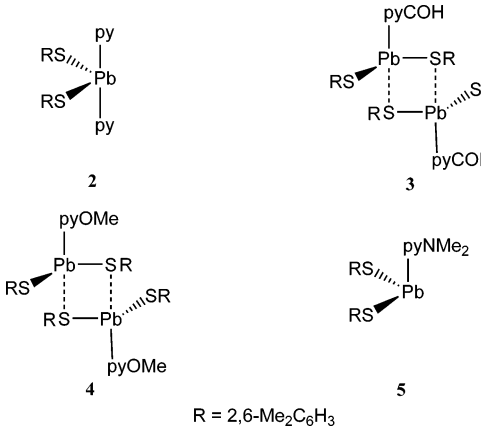

with the thiolate sulfur atoms occupying equatorial positions and the axial amine nitrogen atoms involved in dative bonding interactions. To determine the effect of altering the Lewis basicity of the amine ligand on the coordination geometry of lead(II) in these systems, we have prepared various 4-substituted pyridine adducts of **1**. This has resulted in the isolation of the complexes shown in Chart 1, which have also been characterized with single-crystal X-ray diffraction.

Whereas refined single-crystal X-ray data is used to accurately portray molecular structure, solid-state ^{207}Pb NMR spectra can provide information on the electronic environment of the metal atom and the nature of bonding with surrounding ligands. ^{207}Pb ($I = {}^1/_2$) is the only NMR-active isotope of lead and has a receptivity of 11.8 relative to ^{13}C.[30] The lead chemical shift range is very large, with a difference of approximately 17 000 ppm between lead metal and plumbocene.[31−34] This large chemical shift range is a product of the extremely polarizable lead valence orbitals, which give rise to the large lead chemical shielding anisotropies (CSA) observed in most solid-state ^{207}Pb NMR spectra (with the exception of complexes of high spherical or Platonic symmetry).[31,35] Lead chemical shifts are extremely sensitive to probes of the atomic/molecular environment and subtle molecular changes induced by chemical (e.g., reactions, solvent coordination) and physical changes (e.g., temperature, stress).[31,33,36,37]

(10) Hao, E. C.; Yang, B.; Yu, S.; Gao, M. Y.; Shen, J. C. *Chem. Mater.* **1997**, *9*, 1598.
(11) Meehan, E. J.; Erdmann, D. J. *J. Colloid Interface Sci.* **1977**, *62*, 8.
(12) Yu, D. B.; Wang, D. B.; Meng, Z. Y.; Lu, J.; Qian, Y. T. *J. Mater. Chem.* **2002**, *12*, 403.
(13) Zhao, X. S.; Gorelikov, I.; Musikhin, S.; Cauchi, S.; Sukhovatkin, V.; Sargent, E. H.; Kumacheva, E. *Langmuir* **2005**, *21*, 1086.
(14) Cornacchio, A. L. P.; Jones, N. D. *J. Mater. Chem.* **2006**, *16*, 1171.
(15) Eichhofer, A. *Eur. J. Inorg. Chem.* **2005**, 1683.
(16) Nenadovic, M. T.; Comor, M. I.; Vasic, V.; Micic, O. I. *J. Phys. Chem.* **1990**, *94*, 6390.
(17) Torimoto, T.; Uchida, H.; Sakata, T.; Mori, H.; Yoneyama, H. *J. Am. Chem. Soc.* **1993**, *115*, 1874.
(18) Fleischer, H.; Schollmeyer, D. *Inorg. Chem.* **2004**, *43*, 5529.
(19) Andersen, R. J.; diTargiani, R. C.; Hancock, R. D.; Stern, C. L.; Goldberg, D. P.; Godwin, H. A. *Inorg. Chem.* **2006**, *45*, 6574.
(20) Magyar, J. S.; Weng, T. C.; Stern, C. M.; Dye, D. F.; Rous, B. W.; Payne, J. C.; Bridgewater, B. M.; Mijovilovich, A.; Parkin, G.; Zaleski, J. M.; Penner-Hahn, J. E.; Godwin, H. A. *J. Am. Chem. Soc.* **2005**, *127*, 9495.
(21) Bharara, M. S.; Kim, C. H.; Parkin, S.; Atwood, D. A. *Polyhedron* **2005**, *24*, 865.
(22) Dean, P. A. W.; Vittal, J. J.; Payne, N. C. *Inorg. Chem.* **1985**, *24*, 3594.
(23) Krebs, B.; Brommelhaus, A.; Kersting, B.; Nienhaus, M. *Eur. J. Solid State Inorg. Chem.* **1992**, *29*, 167.
(24) Rae, A. D.; Craig, D. C.; Dance, I. G.; Scudder, M. L.; Dean, P. A. W.; Kmetic, M. A.; Payne, N. C.; Vittal, J. J. *Acta Crystallogr., Sect. B* **1997**, *53*, 457.
(25) Shimoni-Livny, L.; Glusker, J. P.; Bock, C. W. *Inorg. Chem.* **1998**, *37*, 1853.
(26) *The Encyclopedia of Inorganic Chemistry*; Wiley & Sons: Chichester, U.K., 1994; Vol. 4.
(27) Cramer, R. E.; Waddling, C. A.; Fujimoto, C. H.; Smith, D. W.; Kim, K. E. *J. Chem. Soc., Dalton Trans.* **1997**, 1675.
(28) Tsubomura, T.; Ito, M.; Sakai, K. *Inorg. Chim. Acta* **1999**, *284*, 149.
(29) Appleton, S. E.; Briand, G. G.; Decken, A.; Smith, A. S. *Dalton Trans.* **2004**, 3515.
(30) Harris, R. K.; Becker, E. D.; De Menezes, S. M. C.; Goodfellow, R.; Granger, P. *Pure Appl. Chem.* **2001**, *73*, 1795.
(31) Dybowski, C.; Neue, G. *Prog. Nucl. Magn. Reson. Spectrosc.* **2002**, *41*, 153.
(32) Janiak, C.; Schumann, H.; Stader, C.; Wrackmeyer, B.; Zuckerman, J. J. *Chem. Ber./Recl.* **1988**, *121*, 1745.
(33) Kye, Y. S.; Connolly, S.; Herreros, B.; Harbison, G. S. *Main Group Met. Chem.* **1999**, *22*, 373.
(34) *Multinuclear NMR*; Mason, J., Ed.; Plenum Publishing: New York, 1987; pp 305.
(35) Duncan, T., Michael *A Compilation of Chemical Shift Anisotropies*; The Farragut Press: Chicago, 1990.
(36) Zwanziger, J. W.; Werner-Zwanziger, U.; Shaw, J. L.; So, C. *Solid State Nucl. Magn. Reson.* **2006**, *29*, 113.
(37) Hamilton, B. H.; Kelly, K. A.; Wagler, T. A.; Espe, M. P.; Ziegler, C. J. *Inorg. Chem.* **2004**, *43*, 50.

Once relationships have been established between well-characterized molecular structures and lead chemical shielding (CS) tensors then solid-state NMR can be applied for structural determination of complexes for which single-crystal data are not readily available. Given the general insolubility of homoleptic lead(II) thiolate complexes,[22−24] the lability of their coordination complexes,[29] and the well-known sensitivity of lead CS tensors to subtle changes in molecular structure,[31,33,38] solid-state ^{207}Pb NMR should serve as a formidable probe of molecular structure in these systems. To this end, solid-state ^{207}Pb NMR experiments, in tandem with density functional theory (DFT) calculations of CS tensors, are used to measure and theoretically model lead CS tensors and examine their relationships to structure, symmetry, and bonding.

Experimental Section

General Considerations. 2,6-dimethylbenzenthiol (95%), 4-methoxypyridine (97%), 4-pyridine carboxaldehyde (97%), and 4-dimethylaminopyridine (99+%) were used as received from the Aldrich Chemical Co. Lead(II) acetate trihydrate was used as received from Fischer. (2,6-$Me_2C_6H_3S)_2$Pb (**1**) and (2,6-$Me_2C_6H_3S)_2$-Pb(py)$_2$ (**2**) were prepared as reported previously.[29] General characterization methods (NMR, IR, and elemental analysis) are described in the Supporting Information.

Preparation of [(2,6-$Me_2C_6H_3S)_2$Pb(pyCOH)]$_2$ (3). A solution of pyCOH (0.17 g, 1.5 mmol) in toluene (2 mL) was added dropwise to a solution of **1** (0.20 g, 0.40 mmol) in the same solvent (11 mL) to give a clear orange solution. After stirring for 10 min, the reaction was filtered and allowed to stand at 23 °C. After 1 h, the precipitate was collected by filtration to yield **3** as orange crystals (0.11 g, 0.090 mmol, 23%). Anal. Calcd for $C_{44}H_{46}N_2O_2$-Pb_2S_4: C, 44.88; H, 3.95; N, 2.38. Found: C, 44.72; H, 4.00; N, 2.35. Mp 138 °C (d). FTIR (cm^{-1}): 1707 s, 1668 w, 1560 m, 1415 m, 1316 w, 1228 m, 1211 m, 1167 vw, 1048 m, 1005 m. Solution NMR data (thf-d_8, ppm): ^{1}H NMR, δ = 2.55 (s, 12 H, *Me*$_2$C$_6$H$_3$S), 6.69 (t, $^3J_{H,H}$ = 7 Hz, 2 H, Me$_2$C$_6$*H*$_3$S), 7.01 (d, $^3J_{H,H}$ = 7 Hz, 4 H, Me$_2$C$_6$*H*$_3$S), 7.72 (d, $^3J_{H,H}$ = 6 Hz, NC$_5$*H*$_4$COH, 2 H), 8.84 (d, $^3J_{H,H}$ = 6 Hz, 2 H, NC$_5$*H*$_4$COH), 10.03 (s, 1 H, CO*H*C$_5$H$_4$N). ^{13}C{^{1}H} NMR, δ = 23.8 (*Me*$_2$C$_6$H$_3$S), 121.9 (N*C*$_5$H$_4$COH), 124.6 (Me$_2$*C*$_6$H$_3$S), 126.6 (Me$_2$*C*$_6$H$_3$S), 142.0 (N*C*$_5$H$_4$COH), 142.4 (Me$_2$*C*$_6$H$_3$S), 151.1 (NC$_5$H$_4$COH), 191.4 (NC$_5$H$_4$*C*OH).

Preparation of [(2,6-$Me_2C_6H_3S)_2$Pb(pyOMe)]$_2$ (4). A solution of pyOMe (0.18 g, 1.6 mmol) in dichloromethane (3 mL) was added dropwise to a solution of **1** (0.20 g, 0.40 mmol) in the same solvent (2 mL) to give a clear yellow solution. After stirring for 10 min, the reaction sat for 1 h at 23 °C. The resulting precipitate was collected by filtration to yield **4** as yellow crystals (0.075 g, 0.13 mmol, 32%). Anal. Calcd for $C_{44}H_{50}N_2O_2Pb_2S_4$: C, 44.73; H, 4.27; N, 2.37. Found: C, 44.49; H, 4.60; N, 2.34. Mp 155 °C (d). FTIR (cm^{-1}): 1658 m, 1603 vs, 1566 s, 1504 s, 1331 m, 1292 vs, 1255 m, 1205 s, 1117 w, 1049 s, 1028 vs, 1003 s. Solution NMR data (thf-d_8, ppm): ^{1}H NMR, δ = 2.52 (s, 12 H, *Me*$_2$C$_6$H$_3$S), 3.84 (s, 3 H, NC$_5$H$_4$O*Me*), 6.70 (t, $^3J_{H,H}$ = 7 Hz, 2 H, Me$_2$C$_6$*H*$_3$S), 6.89 (d, $^3J_{H,H}$ = 6 Hz, 2 H, NC$_5$*H*$_4$OMe), 7.00 (d, $^3J_{H,H}$ = 7 Hz, 4 H, Me$_2$C$_6$*H*$_3$S), 8.42 (d, $^3J_{H,H}$ = 6 Hz, 2 H, NC$_5$*H*$_4$OMe). ^{13}C{^{1}H} NMR, δ = 23.3 (*Me*$_2$C$_6$H$_3$S), 54.5 (NC$_5$H$_4$O*Me*), 109.7 (N*C*$_5$H$_4$-OMe), 124.5 (Me$_2$*C*$_6$H$_3$S), 125.1 (N*C*$_5$H$_4$OMe), 126.5 (Me$_2$*C*$_6$H$_3$S), 141.9 (Me$_2$*C*$_6$H$_3$S), 150.8 (NC$_5$H$_4$OMe), 165.9 (NC$_5$H$_4$OMe).

Preparation of (2,6-$Me_2C_6H_3S)_2$Pb(pyNMe$_2$) (5). A solution of pyNMe$_2$ (0.20 g, 1.6 mmol) in toluene (4 mL) was added dropwise to a solution of **1** (0.20 g, 0.40 mmol) in the same solvent (5 mL) to give a greenish-yellow solution. After stirring for 10 min, the reaction was filtered and allowed to sit at 23 °C. The precipitate was collected after 1 d to yield **5** as pale yellow crystals (0.16 g, 0.26 mmol, 66%). Anal. Calcd for $C_{23}H_{28}N_2PbS_2$: C, 45.74; H, 4.68; N, 4.64. Found: C, 45.65; H, 4.58; N, 4.42. Mp 90 °C (d). FTIR (cm^{-1}): 1612 vs, 1579 w, 1537 s, 1390 m, 1344 w, 1294 w, 1225 s, 1163 m, 1163 w, 1113 w, 1053 m, 1030 w, 1003 s, 949 w, 893 vw. Solution NMR data (thf-d_8, ppm): ^{1}H NMR, δ = 2.42 (s, 12 H, *Me*$_2$C$_6$H$_3$S), 2.99 (s, 6 H, NC$_5$H$_4$N*Me*$_2$), 6.55 (d, $^3J_{H,H}$ = 7 Hz, 2 H, NC$_5$*H*$_4$NMe$_2$), 6.69 (t, $^3J_{H,H}$ = 7 Hz, 2 H, Me$_2$C$_6$*H*$_3$S), 6.95 (d, $^3J_{H,H}$ = 7 Hz, 4 H, Me$_2$C$_6$*H*$_3$S), 8.21 (d, $^3J_{H,H}$ = 7 Hz, 2 H, NC$_5$*H*$_4$NMe$_2$). ^{13}C{^{1}H} NMR, δ = 23.2 (*Me*$_2$C$_6$H$_3$S), 38.1 (NC$_5$H$_4$N*Me*$_2$), 106.7 (N*C*$_5$H$_4$NMe$_2$), 125.1 (Me$_2$*C*$_6$H$_3$S), 127.9 (Me$_2$*C*$_6$H$_3$S), 143.2 (Me$_2$*C*$_6$H$_3$S), 149.1 (N*C*$_5$H$_4$NMe$_2$), 154.1 (NC$_5$H$_4$NMe$_2$).

X-ray Structural Analysis. Crystals of **3**−**5** were isolated from the reaction mixtures as indicated above. Single crystals of each compound were coated with Paratone-N oil, mounted using a CryoLoop (Hampton Research), and frozen in the cold stream of the goniometer. Data were measured on a Nonius KappaCCD 4-Circle Kappa FR540C diffractometer using monochromated Mo Kα radiation (λ = 0.71073 Å) at −100 °C. Data were collected using φ and/or ω scans.[39] Data reduction was performed with the *HKL DENZO* and *SCALEPACK* software, which corrects for beam inhomogeneity, possible crystal decay, Lorentz, and polarization effects. A multiscan absorption correction was applied (*SCALEPACK*).[40] Transmission coefficients were calculated using *SHELXL97*−*2*.[41,42] The structures were solved by direct methods (*SHELXS-97*) and refined by full-matrix least-squares on F^2 (*SHELXL97*−*2*).[42] The non-hydrogen atoms were refined anisotropically. Hydrogen atoms were included at geometrically idealized positions (C−H bond distances 0.95/0.99 Å) and not refined. The isotropic thermal parameters of the hydrogen atoms were fixed at 1.2 times that of the preceding carbon atom.

Powder X-ray diffraction patterns were collected using a Bruker AXS HI-STAR system using a general area detector diffractions system. Compounds **2**, **4**, and **5** were finely ground, packed into 1.0 mm glass capillary tubes, and flame sealed. The X-ray source employed was Cu Kα radiation (λ = 1.540598 Å) with an area detector using a 2θ range between 4.0 and 65.0°. Powder X-ray diffraction patterns were simulated with the *PowderCell* software package.[43]

Solution ^{207}Pb and Solid-State ^{207}Pb and ^{13}C NMR. Solution ^{207}Pb and solid-state ^{207}Pb and ^{13}C NMR spectra were acquired on a Varian Infinity Plus spectrometer with an Oxford 9.4 T wide-bore magnet [ν_0(^{1}H) = 399.73, ν_0(^{207}Pb) = 83.63, ν_0(^{13}C) = 100.51 MHz]. Lead chemical shifts were referenced to Me$_4$Pb (δ_{iso} = 0.0 ppm) by setting the isotropic shift of a secondary standard of 0.5 M Pb(NO$_3$)$_2$(aq) to −2941.0 ppm.[38] Carbon chemical shifts were referenced to tetramethylsilane (δ_{iso} = 0.0 ppm) by using the high-

(38) Fayon, F.; Farnan, I.; Bessada, C.; Coutures, J.; Massiot, D.; Coutures, J. P. *J. Am. Chem. Soc.* **1997**, *119*, 6837.

(39) Nonius, B. V. *COLLECT data collection software*, 1998.

(40) Otwinowski, Z.; Minor, W. In *Methods Enzymology*: *Macromolecular Crystallography*; Carter, C. W., Sweet, R. M., Eds.; Academic Press: San Diego, 1997; Vol. 276, pp 307.

(41) Altomare, A.; Burla, M. C.; Camalli, M.; Cascarano, G. L.; Giacovazzo, C.; Guagliardi, A.; Moliterni, A. G. G.; Polidori, G.; Spagna, R. *J. Appl. Crystallogr.* **1999**, *32*, 115.

(42) Sheldrick, G. M. *SHELXL97*−*2, Program for the Solution of Crystal Structures*; University of Göttingen: Göttingen, Germany, 1997.

(43) Kraus, W.; Nolze, G. *PowderCell for Windows*, ver. 2.4; Federal Institute for Materials Research and Testing: Berlin, Germany, 2000.

frequency peak of adamantane as a secondary reference (δ_{iso} = 38.56 ppm).[44]

Solution ^{207}Pb NMR spectra were acquired on a 5 mm HXY triple resonance Varian/Chemagnetics probe. All of the solid-state NMR experiments were performed on a double resonance 4 mm HX Varian/Chemagnetics probe. ^{1}H-^{207}Pb variable-amplitude cross-polarization/MAS (VACP/MAS)[45,46] and cross-polarization/Carr−Purcell−Meiboom−Gill (CP/CPMG)[47,48] experiments were optimized on a sample of lead acetate hydrate [$Pb(OAc)_2 \cdot xH_2O$]. All of the ^{1}H-^{207}Pb CP experiments employed 2.0 μs $\pi/2$ proton pulses and Hartman−Hahn matching fields of approximately 55 kHz. Individual CP/CPMG subspectra were co-added to form the total spectrum (Figure S1). Further details on CP/CPMG experiments are given in the Supporting Information (Table S1 and Figure S2). Static CP/CPMG ^{207}Pb NMR patterns were simulated using the WSolids program.[49] ^{1}H-^{207}Pb VACP/MAS spectra were simulated with the *SIMPSON* program.[50] ^{1}H-^{13}C VACP/MAS spectra of complexes **2**, **4**, and **5** are shown in Figure S3. The TPPM decoupling scheme was employed in all of the experiments.[51]

DFT Calculations. Theoretical calculations were performed with the EPR and NMR modules[52−54] of the *Amsterdam Density Functional* (*ADF*) program suite[55−57] on a dual-2.0 GHz Xeon Dell Precision 650 workstation. The VWN−BP functional was used for electron exchange and correlation for all of the calculations.[58−61] Relativistic effects (including spin−orbit) were taken into account with the zeroth-order regular approximation (ZORA).[62−66] In the current version of *ADF*, analysis of the contributions to CS from the mixing of molecular orbitals can only be performed for nonrelativistic calculations. All-electron gauge including atomic orbitals (GIAO)[67] triple-ζ singly polarized and triple-ζ doubly polarized basis sets were employed on all of the atoms for the nonrelativistic calculations and ZORA calculations, respectively. However, the largest basis set available for lead for the nonrelativistic calculations was a frozen-core basis set, where the core was extended to the 4d shell for lead (Pb·4d). All of the calculations were performed using atomic coordinates from single-crystal X-ray structures. All of the calculations employed a discrete molecular unit, except for those upon **4**, for which a dimer was used. Calculations on Me_4Pb (^{207}Pb NMR standard) were performed upon atomic coordinates from the previously published low-temperature (150 K) crystal structure.[68]

Results and Discussion

The persistence of a ψ-trigonal bipyramidal S_2N_2 coordination geometry for lead(II) in pyridine, bipyridine, and pyrazine adducts of $(2,6\text{-}Me_2C_6H_3S)_2Pb$ has prompted us to study the effect of systematically altering the donor ability of pyridine on the coordination chemistry at lead(II) in these systems. Pyridine ligands were chosen because they allow for the fine-tuning of the basicity of the coordinating nitrogen atom through the electron withdrawing/donating effects of the para substituent. Further, their relative electron donor abilities may be determined from gas-phase and aqueous proton affinity (PA) data. All of the prior studies yield the following trend for proton affinity (Lewis basicity) values: $pyNMe_2 > pyOMe > py > pyCHO$.[69−74]

Syntheses and Solution NMR. The reaction of **1** with 4 equivs of the appropriate 4-substituted pyridine in toluene or dichloromethane yielded only 1:1 adducts, namely, **3**, **4**, and **5**, as crystalline solids in moderate yields. These results are in contrast to the isolation of the 1:2 adduct $(2,6\text{-}Me_2C_6H_3S)_2Pb(py)_2$ (**2**) for the unsubstituted pyridine ligand.[29] In the preparation of **2**, however, reaction conditions were significantly different, with the product being isolated from neat pyridine. Attempts to obtain any crystalline material through the reaction of **1** with 4 equivs of pyridine in various organic solvents were unsuccessful. As was previously observed for **2**, solution ^{1}H and ^{13}C{^{1}H} NMR spectra for **3**, **4**, and **5** dissolved in thf-d_8 have similar resonances to those of **1** and the corresponding uncomplexed 4-substituted pyridine ligands. Solution ^{207}Pb NMR spectra of **2**, **4**, and **5** dissolved in thf confirm this hypothesis (Figure S4). Similar ^{207}Pb NMR resonances suggest that the complexes are labile in solution and that their structures only persist in the solid state (Supporting Information).

X-ray Structural Analyses. Crystallographic data is given in Table 1, and selected bond distances and angles are given in Table 2. The structure of **3** has a single unique four-coordinate lead center bonded to two thiolate sulfur atoms [Pb1−S1 = 2.6636(16); Pb1−S2 = 2.6256(17) Å] and a

(44) Earl, W. L.; Vanderhart, D. L. *J. Magn. Reson.* **1982**, *48*, 35.
(45) Peersen, O. B.; Wu, X. L.; Kustanovich, I.; Smith, S. O. *J. Magn. Reson. Ser. A* **1993**, *104*, 334.
(46) Peersen, O. B.; Wu, X. L.; Smith, S. O. *J. Magn. Reson. Ser. A* **1994**, *106*, 127.
(47) Hung, I.; Rossini, A. J.; Schurko, R. W. *J. Phys. Chem. A* **2004**, *108*, 7112.
(48) Siegel, R.; Nakashima, T. T.; Wasylishen, R. E. *J. Phys. Chem. B* **2004**, *108*, 2218.
(49) Eichele, K.; Wasylishen, R. E. *WSolids: Solid-State NMR Spectrum Simulation*, ver. 1.17.30, 2001.
(50) Bak, M.; Rasmussen, J. T.; Nielsen, N. C. *J. Magn. Reson.* **2000**, *147*, 296.
(51) Bennett, A. E.; Rienstra, C. M.; Auger, M.; Lakshmi, K. V.; Griffin, R. G. *J. Chem. Phys.* **1995**, *103*, 6951.
(52) Schreckenbach, G.; Ziegler, T. *J. Phys. Chem.* **1995**, *99*, 606.
(53) Schreckenbach, G.; Ziegler, T. *Int. J. Quantum Chem.* **1997**, *61*, 899.
(54) Wolff, S. K.; Ziegler, T. *J. Chem. Phys.* **1998**, *109*, 895.
(55) Guerra, C. F.; Snijders, J. G.; te Velde, G.; Baerends, E. J. *Theor. Chem. Acc.* **1998**, *99*, 391.
(56) Velde, G. T.; Bickelhaupt, F. M.; Baerends, E. J.; Guerra, C. F.; Van, Gisbergen, S. J. A.; Snijders, J. G.; Ziegler, T. *J. Comput. Chem.* **2001**, *22*, 931.
(57) *ADF2005.01* SCM, Theoretical Chemistry, Vrije Universiteit Amsterdam: The Netherlands.
(58) Becke, A. D. *Phys. Rev. A* **1988**, *38*, 3098.
(59) Perdew, J. P. *Phys. Rev. B* **1986**, *34*, 7406.
(60) Perdew, J. P. *Phys. Rev. B* **1986**, *33*, 8822.
(61) Vosko, S. H.; Wilk, L.; Nusair, M. *Can. J. Phys.* **1980**, *58*, 1200.
(62) Autschbach, J.; Ziegler, T. In *Calculation of NMR and EPR Parameters*; Wiley-VCH: Weinheim, Germany, 2004; p 249.
(63) Autschbach, J. In *Calculation of NMR and EPR Parameters*; Wiley-VCH: Weinheim, Germany, 2004; p 227.
(64) van Lenthe, E.; Baerends, E. J.; Snijders, J. G. *J. Chem. Phys.* **1993**, *99*, 4597.
(65) van Lenthe, E.; Baerends, E. J.; Snijders, J. G. *J. Chem. Phys.* **1994**, *101*, 9783.
(66) van Lenthe, E.; van Leeuwen, R.; Baerends, E. J.; Snijders, J. G. *Int. J. Quantum Chem.* **1996**, *57*, 281.
(67) Ditchfield, R. *Mol. Phys.* **1974**, *27*, 789.
(68) Fleischer, H.; Parsons, S.; Pulham, C. R. *Acta Crystallogr., Sect. E: Struct. Rep. Online* **2003**, *59*, M11.
(69) Arnett, E. M.; Chawla, B.; Bell, L.; Taagepera, M.; Hehre, W. J.; Taft, R. W. *J. Am. Chem. Soc.* **1977**, *99*, 5729.
(70) Aue, D. H.; Bowers, M. T. *Gas Phase Ion Chem.* **1979**, *2*, 1.
(71) Hopkins, H. P.; Alexander, C. J.; Ali, S. Z. *J. Phys. Chem.* **1978**, *82*, 1268.
(72) Kebarle, P. *Annu. Rev. Phys. Chem.* **1977**, *28*, 445.
(73) Taageper, M; Taft, R. W.; Brownlee, R. T.; Beauchamp, J. L.; Holtz, D.; Henderso,Wg. *J. Am. Chem. Soc.* **1972**, *94*, 1369.
(74) Voets, R.; Francois, J. P.; Martin, J. M. L.; Mullens, J.; Yperman, J.; Vanpoucke, L. C. *J. Comput. Chem.* **1989**, *10*, 449.

Table 1. Crystallographic Data for **3**−**5**

	3	**4**	**5**
formula	$C_{44}H_{46}N_2O_2Pb_2S_4$	$C_{44}H_{50}N_2O_2Pb_2S_4$	$C_{23}H_{28}N_2PbS_2$
fw	1177.45	1181.48	603.87
cryst syst	orthorhombic	orthorhombic	monoclinic
space group	*Pbca*	*Pbca*	*C*2/*c*
a (Å)	13.7810(3)	13.5750(1)	28.0430(4)
b (Å)	14.5170(4)	14.6870(1)	9.8580(2)
c (Å)	21.2790(6)	21.9220(2)	18.8720(4)
α (deg)	90	90	90
β (deg)	90	90	116.9971(6)
γ (deg)	90	90	90
V (Å^3)	4257.05(19)	4370.72(6)	4648.61(15)
Z	4	4	8
F(000)	2272	2288	2352
ρ_{calcd}, g cm^{-3}	1.837	1.795	1.725
μ, mm^{-1}	8.134	7.923	7.449
T, K	173(2)	173(2)	173(2)
λ, Å	0.71073	0.71073	0.71073
R1[a]	0.0406	0.0325	0.0335
wR2[b]	0.0696	0.0555	0.0620

[a] $R1 = [\sum||F_o| - |F_c||]/[\sum|F_o|]$ for $[F_o^2 > 2\sigma(F_o^2)]$. [b] $wR2 = \{[\sum w(F_o^2 - F_c^2)^2]/[\sum w(F_o^4)]\}^{1/2}$.

Table 2. Selected Bond Distances (Angstroms) and Angles (Degrees) for **3**−**5**

	3	**4**	**5**
Pb1−S1	2.6636(16)	2.6481(6)	2.6211(12)
Pb1−S2	2.6256(17)	2.6179(7)	2.6070(11)
Pb1−S1*	3.1742(16)	3.2671(6)	
Pb1−N1	2.571(5)	2.497(2)	2.432(3)
S1−Pb1−S2	101.32(5)	99.66(2)	87.55(4)
S1−Pb1−N1	87.37(11)	89.00(5)	86.69(9)
S2−Pb1−N1	87.86(12)	88.89(5)	90.87(9)
S1−Pb1−S1*	74.57(5)	74.957(19)	
S2−Pb1−S1*	94.20(5)	95.16(2)	
N1−Pb1−S1*	161.89(11)	163.89(5)	
Pb1−S1−Pb1*	105.43(5)	105.043(19)	
S1−Pb1−S2−C21	−49.2(2)	48.75(9)	172.91(14)
S2−Pb1−S1−C11	−156.6(2)	159.09(9)	−121.18(16)

pyCHO nitrogen atom [Pb1−N1 = 2.571(5) Å] (Figure 1). The metal center is also bound to a thiolate sulfur atom of a neighboring moiety via a long intermolecular Pb···S1* contact [3.1742(16) Å]. The result is a dimeric structure in which each lead center is in a *ψ*-trigonal bipyramidal S_3N bonding environment. Here, the datively bonded pyCHO nitrogen atom and the weakly coordinated thiolate sulfur atom are in the axial positions, and the two closely bonded thiolate sulfur atoms are in the equatorial positions. The remaining equatorial site is presumably occupied by a sterochemically active lone pair of electrons (vide infra). The structure is significantly distorted from an idealized geometry [N1−Pb1−S1* = 161.89(11); S1−Pb1−S2 = 101.32(5)°]. Comparison of the equatorial Pb−S bond distances shows only a small difference between those to the bridging [Pb1−S1 = 2.6636(16)] and terminal [Pb1−S2 = 2.6256(17) Å] thiolate sulfur atoms.

The 4-methoxypyridine adduct, **4**, crystallizes in the same space group as **3** (*Pbca*) and possesses a similar dimeric structure (Figure 2). As with **3**, the single unique lead center displays a four-coordinate *ψ*-trigonal bipyramidal S_3N bonding environment. The most significant structural changes include a decrease in the lead−pyridine bond distance [Pb1−N1 = 2.497(2) Å] and an increase in the intermolecular Pb1···S1* bond distance [3.2671(6) Å]. The

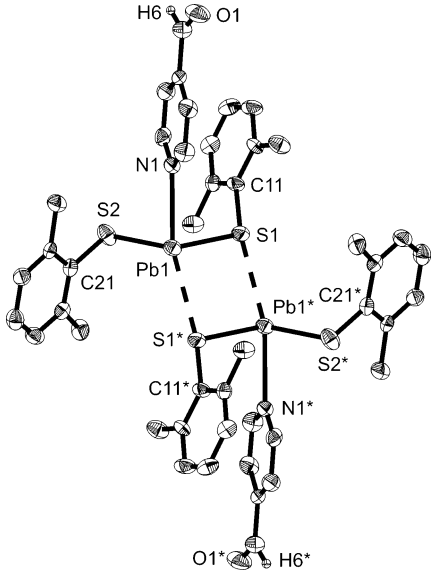

Figure 1. X-ray structure of **3** (30% probability ellipsoids). Hydrogen atoms are removed for clarity. Symmetry transformations used to generate equivalent atoms: (*) $-x + 1, -y + 1, -z + 1$.

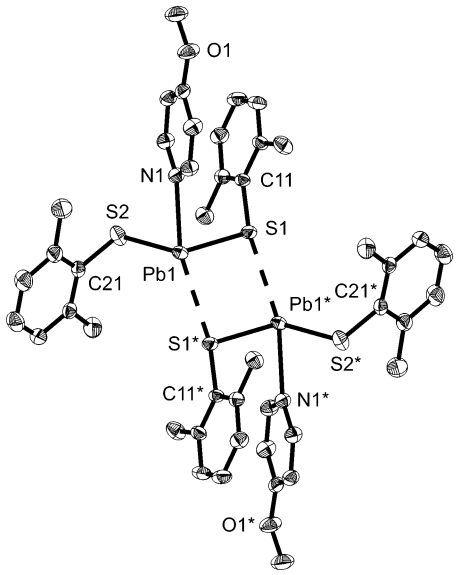

Figure 2. X-ray structure of **4** (30% probability ellipsoids). Hydrogen atoms are removed for clarity. Symmetry transformations used to generate equivalent atoms: (*) $-x + 1, -y + 1, -z + 1$.

latter is accompanied by a slight decrease in the Pb1−S1 (Pb1*−S1*) bond distance [2.6481(6) Å]. Bond angles at the lead(II) center are only slightly different than those in **3** [N1−Pb1−S1* = 163.89(5); S1−Pb1−S2 = 99.66(2)°].

The 4-dimethylaminopyridine adduct, **5**, has a three-coordinate lead center, with a pyridine nitrogen atom [Pb1−N1 = 2.432(3) Å] and two thiolate sulfur atoms [Pb1−S1 = 2.6211(12) and Pb1−S2 = 2.6070(11) Å] (Figure 3). The N−Pb−S [86.69(9) and 90.87(9)°] and S−Pb−S [87.55(4)°] bond angles support a pyramidal geometry, which may be described as *ψ*-trigonal pyramidal, if a basal stereochemically active lone pair is considered (vide infra). Unlike **3** and **4**, compound **5** is monomeric with no intermolecular Pb···S contacts and crystallizes in a different space group (*C*2/*c*). The shortest intermolecular distance is

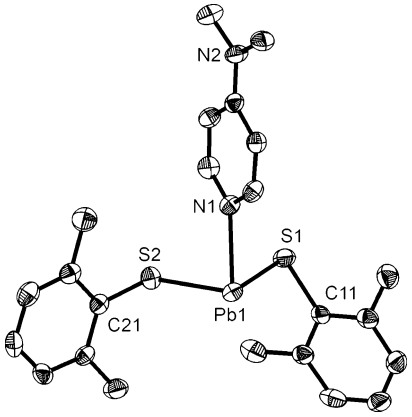

Figure 3. X-ray structure of **5** (30% probability ellipsoids). Hydrogen atoms are removed for clarity.

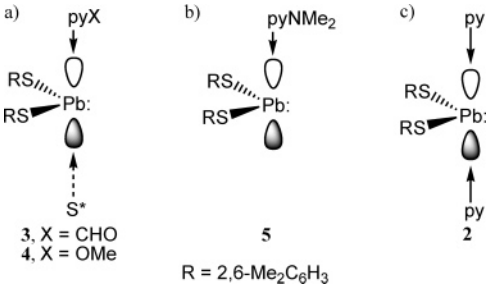

Figure 4. Valence bond descriptions for a) compounds **3** and **4**, b) compound **5**, and c) compound **2**.

between neighboring lead atoms [Pb1···Pb1* = 4.249(1) Å] and is outside the sum of the van der Waals radii (4.0 Å).[75,76]

The relative Lewis basicities of the pyridine ligands and a simple valence bond model (Figure 4) may be used to rationalize the observed structures of **3**, **4**, and **5**. First, it should be noted that the Pb1−N1 bond distances in the structures of **3** [2.571(5)], **4** [2.497(2)], and **5** [2.432(3) Å] decrease as the Lewis basicity of the corresponding 4-substituted pyridine ligands is increased: $pyNMe_2$ > pyOMe > pyCHO. Second, the pyridine nitrogen and *trans*-thiolate sulfur atoms (N1 and S1*, respectively) in compounds **3** and **4** may be viewed as axially coordinating to the $(2,6\text{-}Me_2C_6H_3S)_2Pb$ unit via the empty p orbital on the lead(II) atom, yielding a three-center four-electron bond and a ψ-trigonal bipyramidal S_3N bonding environment (part a of Figure 4). As a consequence of the resulting trans influence, the intermolecular Pb1···S1* bond distance increases [**3**, 3.1742(16); **4**, 3.2671(6) Å] as the Pb1−N1 bond distance decreases. In compound **5**, the Pb1−N1 bond appears to be strong enough to preclude the formation of a trans Pb···S interaction to the Lewis-acidic lead center, resulting in a S_2N bonding environment and a monomeric structure (part b of Figure 4). A similar bonding model may also be used to describe the ψ-trigonal bipyramidal S_2N_2 structure of the bis-pyridine adduct **2**, which involves the coordination of two pyridine ligands via an empty 6p orbital of lead(II) (part c of Figure 4).[29] The Pb−N bond distances [2.695(3) and 2.689(3) Å] are longer than expected, given

Table 3. Experimental ^{207}Pb Chemical Shift Parameters

compound	δ_{11} (ppm)[a]	δ_{22} (ppm)	δ_{33} (ppm)	δ_{iso} (ppm)[b]	Ω (ppm)[c]	κ[d]
2	4814	3286	114	2733(5)[e]	4700(100)	0.35(7)
4	4256	4022	356	2873(5)	3900(100)	0.88(10)
5	4519	4024	19	2852(5)	4500(100)	0.78(15)

[a] The chemical shift tensor is described by three principal components ordered such that $\delta_{11} \geq \delta_{22} \geq \delta_{33}$. Shift values for the individual components are calculated from the values of Ω, κ, and δ_{iso}. [b] $\delta_{iso} = (\delta_{11} + \delta_{22} + \delta_{33})/3$. δ_{iso} is given relative to $(CH_3)_4Pb$ [$\delta_{iso}(^{207}Pb) = 0.0$ ppm]. All of the values are taken from VACP/MAS NMR spectra acquired at a spinning speed of 5000 Hz. [c] $\Omega = \delta_{11} - \delta_{33}$. On the basis of simulations of the static CP/CPMG spectra. [d] $\kappa = 3(\delta_{22} - \delta_{iso})/\Omega$, $-1.0 \leq \kappa \leq +1.0$. On the basis of simulations of the static CP/CPMG spectra. [e] The uncertainty in the last digit of each value is denoted in brackets. Error bounds in the principle CS tensor components (eg., δ_{11}) are of a similar magnitude to those of Ω.

Chart 2. Schematic Drawing of the Bicyclic Aminoethanethiolate Complex $(H_2NCH_2CH_2S)_2Pb$

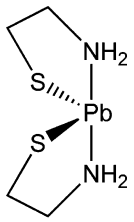

6

the relative Lewis basicity of the unsubstituted pyridine (vide supra). This observation is likely a result of the strong trans influence of the two axial pyridine ligands. The structure also exhibits shorter equatorial Pb−S bond distances [2.6078(9) and 2.6079(9) Å] than observed in compounds **3**, **4**, and **5**.

Ab initio calculations for the bicyclic aminoethanethiolate complex $(H_2NCH_2CH_2S)_2Pb$ (**6**), which exhibits a S_2N_2 ψ-trigonal bipyramidal bonding environment via intramolecular Pb−N interactions (Chart 2), suggest that n_p(S) and n(N) compete for interaction with the 6p(Pb) orbital.[18] Although the S−Pb−S−C torsion angles in **3** and **4** deviate significantly from 0 or 180° (Table 2), indicating minimal π-type n_p(S)-6p(Pb) interaction, the S1−Pb1−S2−C21 torsion angle of compound **5** [172.91(14)°] is very close to 180°. This may indicate that such an interaction is significant in precluding the Pb···S* bond formation.

Solid-State ^{207}Pb NMR Spectroscopy. In this section, we discuss the acquisition and interpretation of solid-state ^{207}Pb NMR spectra of complexes **2**, **4**, and **5**, to examine the electronic structure, bonding environment at the lead center, and presence and/or influence of the lone pair of electrons on the lead CSA. In many cases, it has been observed that the direct detection of ^{207}Pb NMR spectra in solids is challenging, because the ^{207}Pb longitudinal relaxation times (T_1) may be very long.[38,77−79] To circumvent the long

(75) Bondi, A. *J. Phys. Chem.* **1964**, *68*, 441.
(76) Brown, I. D. *Chem. Soc. Rev.* **1978**, *7*, 359.
(77) Grutzner, J. B.; Stewart, K. W.; Wasylishen, R. E.; Lumsden, M. D.; Dybowski, C.; Beckmann, P. A. *J. Am. Chem. Soc.* **2001**, *123*, 7094.
(78) Zhao, P. D.; Prasad, S.; Huang, J.; Fitzgerald, J. J.; Shore, J. S. *J. Phys. Chem. B* **1999**, *103*, 10617.
(79) Van, Bramer, S. E.; Glatfelter, A.; Bai, S.; Dybowski, C.; Neue, G.; Perry, D. L. *Magn. Reson. Chem.* **2006**, *44*, 357.

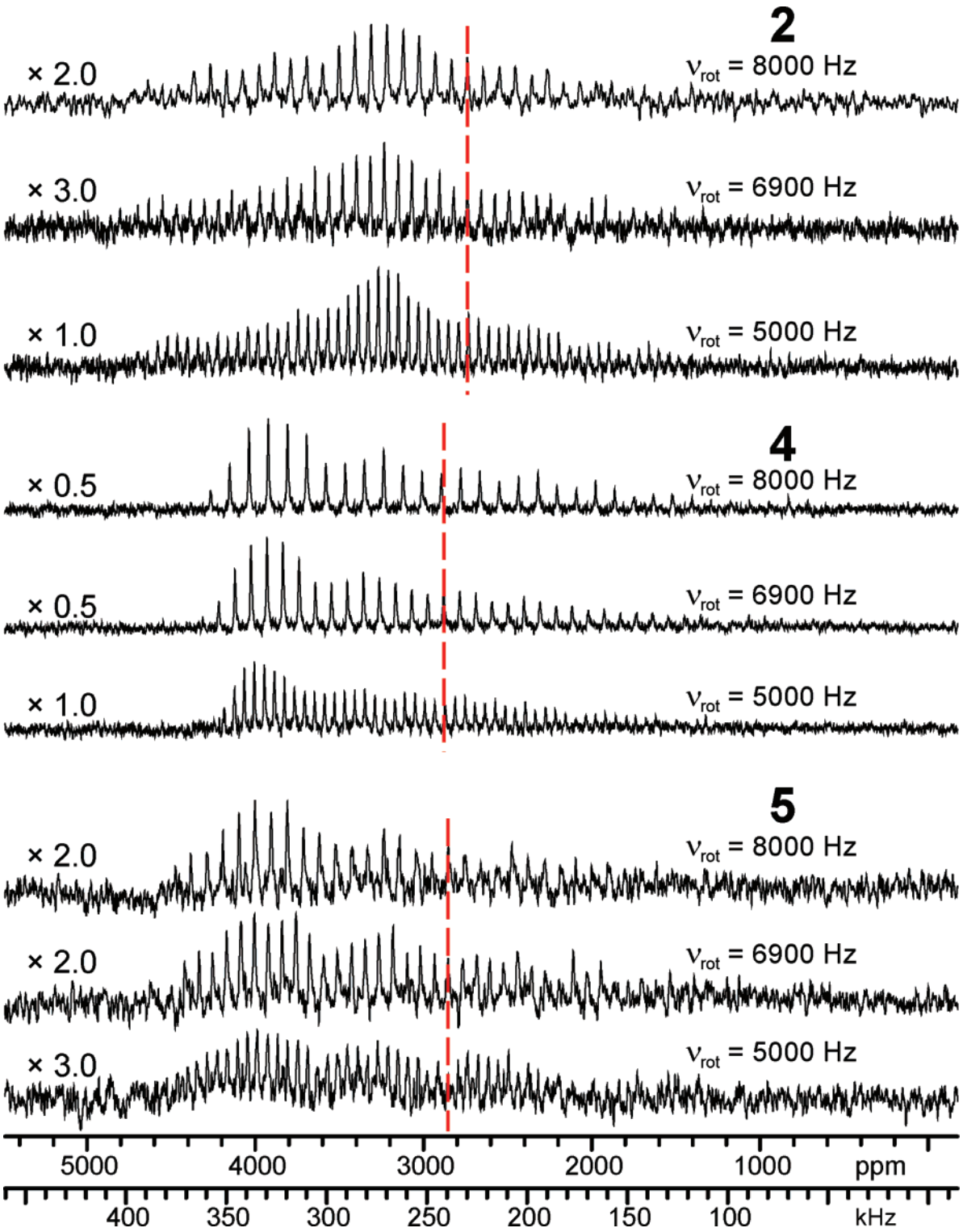

Figure 5. ^{1}H-^{207}Pb VACP/MAS NMR spectra of **2**, **4**, and **5**, each acquired at three spinning speeds (ν_{rot}). Dashed lines indicate δ_{iso}. A recycle delay of 10 s was used for all of the spectra and 2004 to 8428 scans were acquired. The relative vertical scaling of the spectra is given on the left.

^{207}Pb T_1 constants, ^{1}H-^{207}Pb variable-amplitude cross-polarization (VACP/MAS) NMR experiments[45,46] were performed on compounds **2**, **4**, and **5** (Figure 5). Normally, only two spinning speeds are required to differentiate peaks as a result of spinning sidebands from that of the isotropic chemical shift in the MAS NMR spectra of a spin $^{1}/_{2}$ nucleus. However, the overlap of spinning sidebands due to large spans (Ω, defined in Table 3) requires that the spectrum be acquired at three different spinning speeds (expanded views of the spectra are given in Figure S5). The isotropic shifts in this series of complexes are similar to those reported from solution ^{207}Pb NMR experiments on $[(PhS)_3Pb][Ph_4As]$, δ_{iso} = 2868 ppm,[80] which has an S_3 lead coordination environ-

(80) Dean, P. A. W.; Vittal, J. J.; Payne, N. C. *Inorg. Chem.* **1984**, *23*, 4232.

ment, but are clearly distinct from the S_2N environment in [PATH−Pb][ClO_4], for which $\delta_{iso} = 2358$ ppm.[19]

A temperature-dependent chemical shift is observed for compounds **2** and **4** (Figure S5 and Table S2). This behavior is well-known and was previously observed in the ^{207}Pb NMR spectra of $Pb(NO_3)_2$,[81−85] among other lead-containing systems. Minor impurity peaks are visible in the VACP/MAS NMR spectra and are attributed to hydration of the samples because the MAS spectra were acquired *after* the static NMR and powder X-ray diffraction experiments (Figure S6). Relatively accurate values for δ_{iso} (Table 3) can be obtained from the VACP/MAS spectra; however, the large number of spinning sidebands and the poor signal-to-noise of the spectra make extraction of the CS tensor parameters by the Herzfeld−Berger analysis difficult and potentially inaccurate.

With this in mind, static (i.e., stationary sample) ^{1}H-^{207}Pb cross-polarization/Carr−Purcell−Meiboom−Gill (CP/CP-MG) experiments were performed.[47,48,86−88] Because of the large breadth of the lead powder patterns, the entire spectrum must be acquired in a piecewise frequency offset fashion (Figure S1), which requires both constant resetting of the transmitter frequency and probe retuning. The appearance of spikelets in the frequency domain spectra arise from the Fourier transform of the CPMG echo train (alternatively and completely equivalently, one may co-add the echoes and process the summed spin echo to produce a static pattern). Acquisition of static CP/CPMG spectra is not hindered by a partial averaging of the ^{1}H-^{207}Pb dipolar interactions that would occur under MAS conditions; hence, high signal-to-noise static patterns can be acquired very rapidly with respect to VACP/MAS NMR spectra of the same quality. Another clear advantage of the CP/CPMG experiments over their VACP/MAS counterparts is the overall excitation of the ^{207}Pb NMR powder patterns. Simulations of the VACP/MAS spectra that employ the CS tensor parameters extracted from the CP/CPMG spectra (vide infra) clearly demonstrate that the former are not uniformly excited and are unsuitable candidates for the accurate measurement of CS tensor parameters via Herzfeld−Berger methods (Figure S7). This is in contrast to direct excitation and detection of broad ^{207}Pb NMR powder patterns. For instance, Antzutkin et al. recently measured and simulated ^{207}Pb MAS NMR spectra of lead patterns with spans close to 4000 ppm and breadths of ca. 300 kHz (acquisition times of ca. 24−48 h).[89]

Co-addition of the subspectra and simulation of the observed patterns (Figure 6) yield the lead CS tensor parameters (Table 3). The δ_{iso} is located at the center of gravity of the powder pattern. The Ω and κ describe the breadth of anisotropic chemical shifts (i.e., the size of the CSA) and the degree of axial symmetry of the CS tensor. Though the CS tensor parameters are distinct (Table 3), they do not vary widely in this series of complexes. This suggests that the orientations of the CS tensors in the molecular frames are related among the three complexes and that the general modes of bonding and electronic environments at the lead centers are very similar. However, there are some interesting trends in these parameters which can be correlated to molecular structure and symmetry.

First, all three patterns have extremely large spans (Table 3). The Ω values observed for complexes **2** and **5** are several hundred ppm larger than those observed for yellow lead oxide ($\Omega = 3917$ to 3995 ppm) and lead(II) dialkyldithiophosphates ($\Omega = 3840$ ppm), which, to the best of our knowledge, are the largest spans previously reported for lead complexes.[33,38,78,89] Second, all of the patterns possess positive skews, denoting δ_{33} as the distinct component in each case, and implying that it must be oriented in a distinct/unique environment within the molecule. Positive skews have previously been observed in the ^{207}Pb NMR spectra of several lead(II) complexes, which are also thought to have an electron lone pair molecular orbital (MO) localized at the lead centers.[33,37,38,78] Because it is well-known that CS tensor components orient along/near symmetry elements, and by virtue of the fact that the δ_{33} is the distinct component in each complex, it is very likely that δ_{33} is oriented along/near the direction of the presumed lone pair of electrons (contained within the PbS_2 plane, Figure 4). Finally, despite the similarity of the isotropic shifts of **4** and **5**, the spectra of their respective S_3N and S_2N metal bonding environments are readily distinguished by the differences in Ω and κ (this is visually apparent in comparing these spectra as well, Figure 6). With this limited set of structural parameters and NMR data, two observations can be made: (i) decreased Pb−S bond lengths are correlated with larger spans and (ii) the unique four-coordinate S_2N_2 environment of **2** leads to a less-axial CS tensor.

Theoretical Calculations of Lead CS Tensors. Ab initio and/or pure DFT computational methods can be used to calculate the CS tensor parameters, their orientations within the molecular frames, and contributions from individual MOs. Ramsey's theory of magnetic shielding arbitrarily decomposes the total magnetic shielding (σ) at a nucleus into diamagnetic and paramagnetic terms, such that $\sigma = \sigma_d + \sigma_p$.[90−95] The diamagnetic and paramagnetic terms arise from the circulation of electrons in ground state MOs and the mixing of separate MOs, respectively, both of which are induced by the presence of an external magnetic field. Ziegler and co-workers have developed a DFT-GIAO formalism for the calculation of magnetic shielding, which further parti-

(81) Bielecki, A.; Burum, D. P. *J. Magn. Reson. Ser. A* **1995**, *116*, 215.
(82) Ferguson, D. B.; Haw, J. F. *Anal. Chem.* **1995**, *67*, 3342.
(83) Mildner, T.; Ernst, H.; Freude, D. *Solid State Nucl. Magn. Reson.* **1995**, *5*, 269.
(84) Neue, G.; Dybowski, C. *Solid State Nucl. Magn. Reson.* **1997**, *7*, 333.
(85) Van, Gorkom, L. C. M.; Hook, J. M.; Logan, M. B.; Hanna, J. V.; Wasylishen, R. E. *Magn. Reson. Chem.* **1995**, *33*, 791.
(86) Carr, H. Y.; Purcell, E. M. *Phys. Rev.* **1954**, *94*, 630.
(87) Meiboom, S.; Gill, D. *Rev. Sci. Instrum.* **1958**, *29*, 688.
(88) Larsen, F. H.; Jakobsen, H. J.; Ellis, P. D.; Nielsen, N. C. *J. Phys. Chem. A* **1997**, *101*, 8597.
(89) Larsson, A. C.; Ivanov, A. V.; Pike, K. J.; Forsling, W.; Antzutkin, O. N. *J. Magn. Reson.* **2005**, *177*, 56.
(90) Autschbach, J. In *Principles and Applications of Density Functional Theory in Inorganic Chemistry I*; Kaltsoyannis, N., McGrady, J. E., Eds.; Springer Publishing: New York, 2004; Vol. 112, p 1.
(91) de Dios, A. C. *Prog. Nucl. Magn. Reson. Spectrosc.* **1996**, *29*, 229.
(92) Fukui, H.; Baba, T.; Inomata, H. *J. Chem. Phys.* **1996**, *105*, 3175.
(93) Ramsey, N. F. *Phys. Rev.* **1950**, *78*, 699.
(94) Ramsey, N. F. *Phys. Rev.* **1951**, *83*, 540.
(95) Ramsey, N. F. *Phys. Rev.* **1952**, *86*, 243.

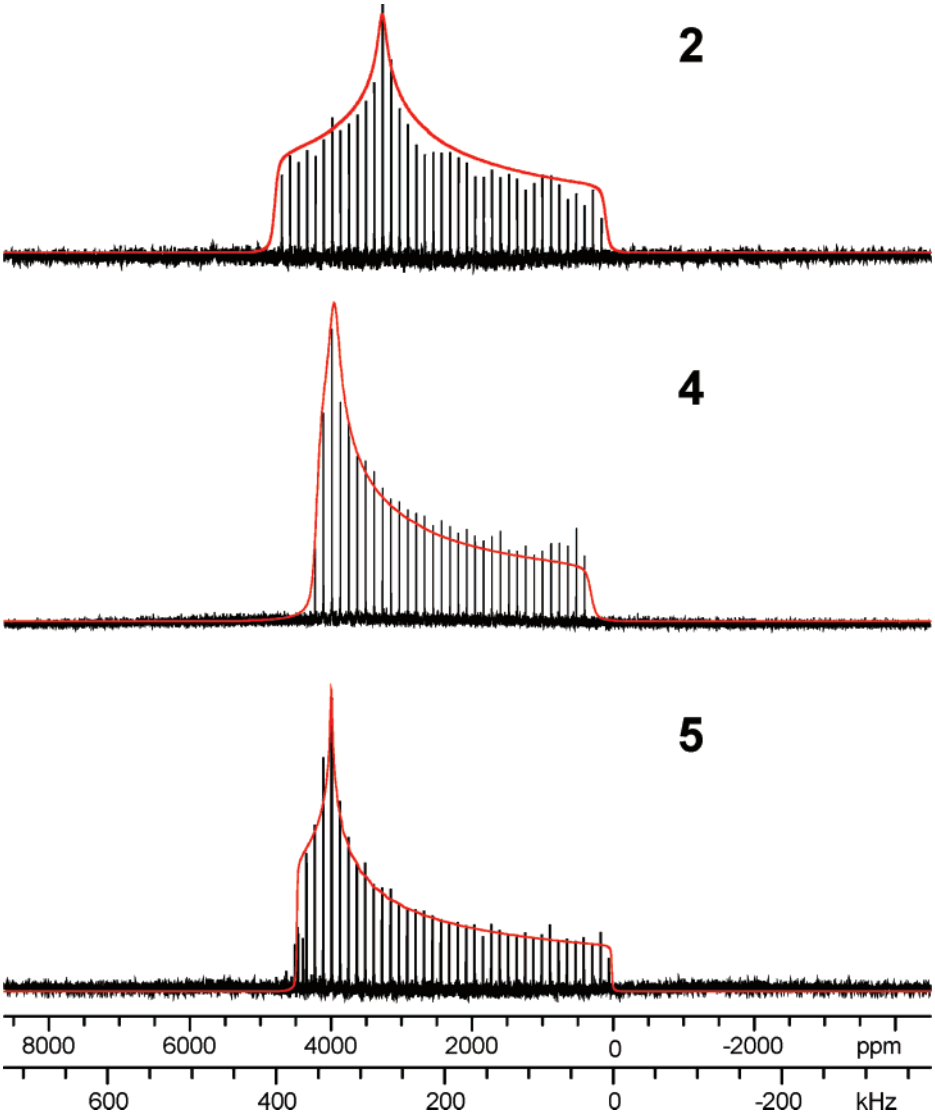

Figure 6. ^{1}H-^{207}Pb CP/CPMG static NMR spectra and WSolids simulations of compounds **2**, **4**, and **5**. The CS tensor parameters obtained from the simulations can be found in Table 3.

tions the paramagnetic terms into contributions from the mixing of occupied MOs ($\sigma_p^{occ-occ}$) and the mixing of occupied and virtual MOs ($\sigma_p^{occ-vir}$),[52−54] the details of which are neatly summarized elsewhere.[96] Furthermore, for heavy nuclei (^{207}Pb, ^{195}Pt, etc.), it is often necessary to include the relativistic contributions to the total shielding as described by the spin−orbit coupling term (σ_{so}) to improve agreement between experiment and theory.[53,62,63,90,97−103]

Lead chemical shielding parameters from calculations performed with the *ADF* program suite incorporating ZORA[64−66] are shown in Table 4. In each case, the ZORA calculations yield values of κ, which are in good agreement with experimental values. Theoretical values of Ω are lower than experimental values in each case, which arise from consistent underestimation of deshielding along the directions of σ_{11} and σ_{22}. The errors in the calculated σ_{11} and σ_{22} parameters are unsurprising, given the difficulties associated with accurately calculating the excited electronic states of larger molecules containing lead atoms. Because the chemical shift range of lead is approximately 17 000 ppm, and the spans of the CS tensors are so large, these errors are relatively small (ranging from 15 to 30%). The calculations also qualitatively predict the relative values of δ_{iso} (the ^{207}Pb nucleus in **2** is predicted to be the most shielded and that in **4** is predicted to be the least shielded). While the theoretical tensors are not identical to the experimental measurements, they are still extremely useful in understanding the origin of the lead CS in these systems.

Contributions to the principal shielding components of the total shielding tensor have been tabulated for the diamagnetic,

(96) Harris, K. J.; Bernard, G. M.; McDonald, C.; McDonald, R.; Ferguson, M. J.; Wasylishen, R. E. *Inorg. Chem.* **2006**, *45*, 2461.
(97) Willans, M. J.; Demko, B. A.; Wasylishen, R. E. *Phys. Chem. Chem. Phys.* **2006**, *8*, 2733.
(98) Bagno, A.; Casella, G.; Saielli, G. *J. Chem. Theory Comput.* **2006**, *2*, 37.
(99) Jokisaari, J.; Jarvinen, S.; Autschbach, J.; Ziegler, T. *J. Phys. Chem. A* **2002**, *106*, 9313.
(100) Bryce, D. L.; Wasylishen, R. E.; Autschbach, J.; Ziegler, T. *J. Am. Chem. Soc.* **2002**, *124*, 4894.
(101) Rodriguez-Fortea, A.; Alemany, P.; Ziegler, T. *J. Phys. Chem. A* **1999**, *103*, 8288.
(102) Autschbach, J.; Ziegler, T. *J. Chem. Phys.* **2000**, *113*, 9410.
(103) Autschbach, J.; Ziegler, T. *J. Chem. Phys.* **2000**, *113*, 936.

Table 4. ZORA and Nonrelativistic (NR) *ADF* Calculations of ^{207}Pb CS Tensor Parameters

complex	method	shielding term	σ_{11} (ppm)[a]	σ_{22} (ppm)	σ_{33} (ppm)	σ_{iso} (ppm)	δ_{iso} (ppm)[a]	Ω (ppm)	κ
$(CH_3)_4Pb$	ZORA	Total	7523.7	7523.8	7546.5	7531.0	0.0	22.8	1.00
	NR	Total	5447.1	5453.0	5453.0	5451.1	0.0	5.9	−0.99
2	Exptl	Total[b]	2717	4245	7417	4793	2733	4700	0.35
	ZORA	Total	4252.6	5301.0	7631.2	5728.27	1803.1	3378.6	0.38
		σ_d	9949.2	9946.1	9940.4	9945.2		−8.8	
		σ_p	−6448.7	−5440.1	−4768.1	−5552.3		1680.6	
		σ_{so}	752.1	795.1	2458.9	1335.3		1706.8	
	NR	Total	5131.6	5771.9	6453.9	5785.8	−334.7	1322.3	0.03
		σ_d	10 062.3	10 059.5	10 052.2	10 058.0		−10.1	
		σ_p	−4930.7	−4287.6	−3598.2	−4272.2		1332.5	
4	Exptl	Total	3275	3509	7175	4653	2873	3900	0.88
	ZORA	Total	4217.4	4341.2	7382.2	5313.6	2217.8	3164.9	0.92
		σ_d	9948.8	9947.6	9941.4	9945.9		−7.4	
		σ_p	−6501.1	−6099.9	−4758.5	−5786.5		1742.6	
		σ_{so}	769.7	493.6	2199.4	1154.2		1429.7	
	NR	Total	5146.9	5231.3	6387.5	5588.6	−137.5	1240.6	0.87
		σ_d	10 058.7	10 062.6	10 052.9	10 058.0		−5.8	
		σ_p	−4911.7	−4831.3	−3665.3	−4469.5		1246.4	
5	Exptl	Total	3012	3507	7512	4677	2852	4500	0.78
	ZORA	Total	3998.3	4341.1	7778.2	5372.5	2158.8	3780.0	0.82
		σ_d	9948.5	9947.0	9943.2	9946.2		−5.3	
		σ_p	−6729.2	−6339.1	−4559.0	−5875.8		2170.2	
		σ_{so}	779.0	733.2	2394.0	1302.1		1615.0	
	NR	Total	4747.2	5256.2	6473.9	5492.4	−41.3	1726.7	0.41
		σ_d	10 060.8	10 060.7	10 056.5	10 059.3		−4.3	
		σ_p	−5313.6	−4804.5	−3582.6	−4566.9		1731.0	

[a] The CS tensor is described by three principal components ordered such that $\sigma_{11} \leq \sigma_{22} \leq \sigma_{33}$ (highest to lowest chemical shift). The principal chemical shift components (δ_{jj}) are related to the principal chemical shielding components (σ_{jj}) by the equation $\delta_{jj} = (\sigma_{iso,\,ref} - \sigma_{jj})(10^6)/(1 - \sigma_{iso,\,ref}) \approx \sigma_{iso,ref} - \sigma_{jj}$, where $jj = 11$, 22, or 33 and $\sigma_{iso,ref}$ refers to the isotropic shielding value of the reference compound ($\sigma_{iso,ref} = \sigma_{iso}(Me_4Pb)$). [b] The experimental shift values have been converted to shielding values by subtracting them from the ZORA-calculated value of $\sigma_{iso}(Me_4Pb)$; $\sigma_{jj} = 7531.0 - \delta_{jj}$.

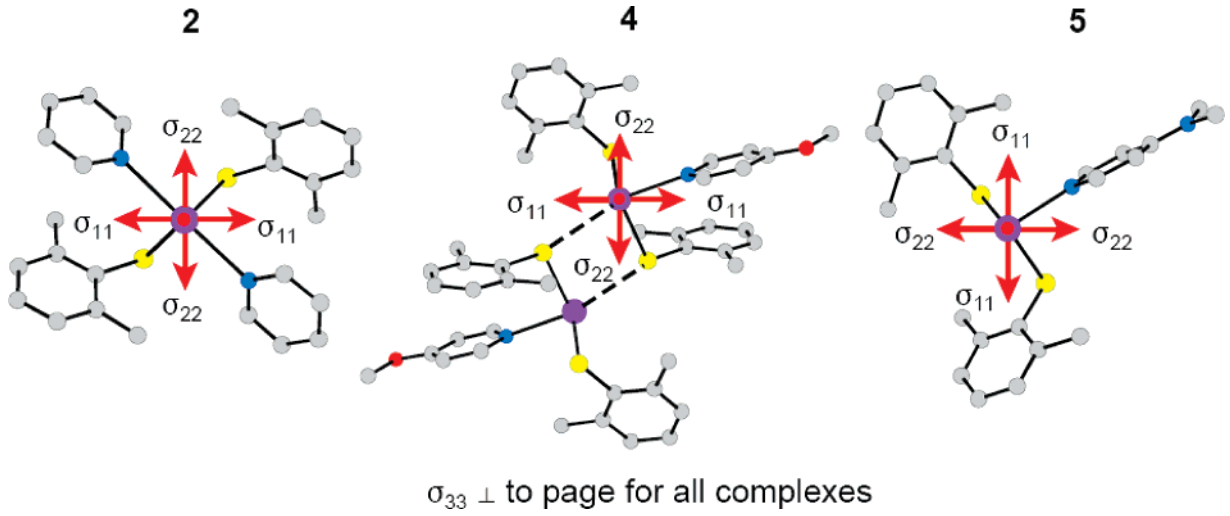

Figure 7. Lead CS tensor orientations for complexes **2**, **4**, and **5**. The tensor orientations have been generated from the ZORA calculations.

paramagnetic, and spin−orbit terms for each compound (Table 4 and Supporting Information). The diamagnetic terms for each compound are highly isotropic (small Ω values) and do not contribute to the large shielding anisotropies. The paramagnetic term makes much larger contributions to the isotropic shielding values than the spin−orbit term, but both terms contribute relatively equally to the spans of the CS tensors. Comparison of the ZORA and nonrelativistic (NR) calculations makes it very clear that the inclusion of relativistic effects for the calculations of CS tensors for heavy nuclei is absolutely necessary.

The nature of the CS tensor (i.e., the large span and the positive skews) and its relationship to molecular structure can be rationalized by considering the orientation of the CS tensor in the molecular frame (Table S3). The lead CS tensor orientations generated from the ZORA calculations are presented in Figure 7 for complexes **2**, **4**, and **5**. In all three systems, the σ_{33} component is oriented in the presumed direction of the stereochemically active lone pair and close to the plane of the S−Pb−S bonding arrangement. Conversely, the σ_{11} and σ_{22} components are not directed along Pb−S or Pb−N bonds and are oriented as such because of large paramagnetic deshielding contributions arising from the mixing of occupied MOs localized on lead, sulfur, and nitrogen atoms with an assortment of low-lying virtual MOs.

Table 5. Contributions to Paramagnetic Shielding from Mixing of occ-vir MOs in **2**

occupied MO	σ_{iso} from occ MO (ppm)[a]	Sum of σ_{iso} (ppm)	major occ−vir Pairs	σ_{iso} of MO pair (ppm)	σ_{11} (ppm)	σ_{22} (ppm)	σ_{33} (ppm)
1 to 120	−332.7	−332.7					
121	−399.0	−731.7					
122	−323.8	−1055.5	122−138	−81.6	−11.5	−219.6	−13.6
			122−143	−76.4	−27.6	−19.8	−181.8
			Sum	−158.0	−39.1	−239.4	−195.4
123 and 124	−6.3	−1061.7					
125	−428.2	−1489.9	125−143	−135.6	−10.8	−6.7	−389.4
126	−467.5	−1957.4	126−143	−124.8	−318.0	−65.2	8.8
127 to 129	−3.1	−1960.6					
130	−894.7	−2854.3	130−138	−451.4	−468.9	−816.9	−68.3
			130−139	−78.3	12.9	−16.2	−231.5
			130−144	−84.0	−54.4	−156.4	−41.4
			Sum	−613.7	−510.4	−989.5	−341.2
131	−461.8	−3316.0	131−138	−88.6	54.1	−281.7	−38.2
			131−139	199.2	78.5	546.9	−27.8
			131−140	−84.8	−3.2	−315.0	63.8
			131−143	−256.9	−314.5	126.2	−582.5
			Sum	−231.1	−185.1	76.4	−584.7
132	−240.6	−3556.6	132−138	−451.2	−105.5	−1216.4	−31.5
			132−142	−78.9	−86.1	18.3	−169.2
			132−143	231.7	172.6	145.8	376.6
			Sum	−298.4	−19.0	−1052.3	175.9
133 (HOMO)	−308.5	−3865.1	133−139	430.4	45.5	1271.4	−25.8
			133−143	−611.8	−1210.8	−691.5	66.9
			Sum	−181.4	−1165.3	579.9	41.1
			Total	−1743.0	−2247.4	−1696.8	−1284.9

[a] This column corresponds to the sum of the isotropic shieldings of the occ-vir MO pairs that contain the specified occ MO.

Our hypotheses regarding both the large spans and the high positive skews and their relation to molecular structure can be confirmed by analyzing the contributions made by individual MOs to the paramagnetic shielding terms. Analyses of the contributions of particular MOs to paramagnetic shielding in simple molecular systems have previously been demonstrated using both the *Gaussian* software package[104−106] and the *ADF* software.[52,96,107,108] The NMR/EPR module of the *ADF* program suite outputs the paramagnetic shielding contributions arising from mixing of individual occupied−virtual (occ−vir) and occupied−occupied (occ−occ) MO pairs. However, this analysis is only available for NR calculations in the current implementation of *ADF*. Despite the fact that the NR calculations show poor quantitative agreement with experiment, the paramagnetic contributions and CS tensor orientations are very similar to those generated from ZORA calculations (Figure S8). Hence, it is reasonable to examine individual contributions from MO pairs to the paramagnetic terms of the lead CS tensor.

As a result of the relatively high local symmetry at the lead atom in complex **2**, we have chosen this as the focus of our discussion of MO contributions to magnetic shielding (a full MO analysis for all of the systems is beyond the scope of the current article). The contributions from the mixing of occupied (occ) and virtual (vir) MOs in complex **2** are summarized in Table 5 (these MOs are depicted in Figures 8 and S9) and account for upward of 90% of the total isotropic shielding contribution from the paramagnetic term. Therefore, occ−occ mixing will not be considered. As a result of the enormous number of MO pairs, only those contributing greater than 2% (∼77 ppm) of the total isotropic shielding contribution of occ−vir MO mixing (−3865.1 ppm) are listed. In this way, analysis of MO contributions to paramagnetic shielding can be focused upon a select few MOs that are near the HOMO and/or involved in metal−

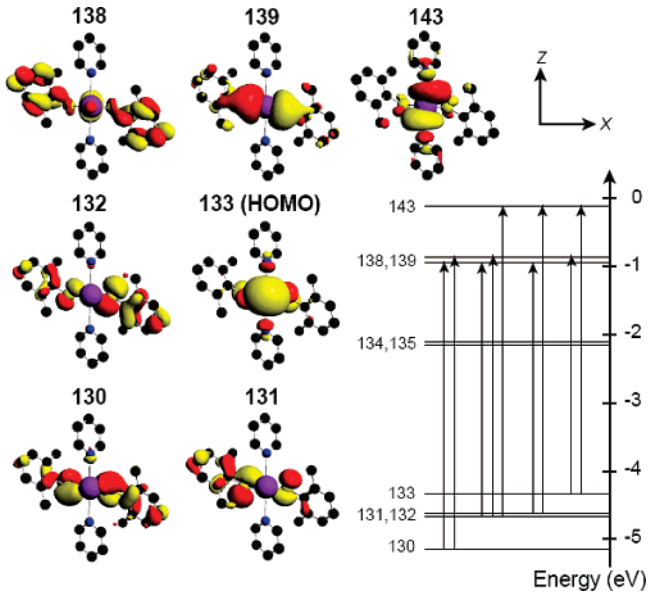

Figure 8. The occupied and virtual MOs of **2** that make significant contributions to the paramagnetic shielding term. A partial MO diagram indicating the magnetic dipole allowed transitions between the occupied and virtual orbitals that are pictured, is also shown. The MOs are visualized at the 97% electron density level.

(104) Wiberg, K. B.; Hammer, J. D.; Keith, T. A.; Zilm, K. *J. Phys. Chem. A* **1999**, *103*, 21.
(105) Wiberg, K. B.; Hammer, J. D.; Zilm, K. W.; Cheeseman, J. R. *J. Org. Chem.* **1999**, *64*, 6394.
(106) Wiberg, K. B.; Hammer, J. D.; Zilm, K. W.; Cheeseman, J. R.; Keith, T. A. *J. Phys. Chem. A* **1998**, *102*, 8766.
(107) Forgeron, M. A. M.; Wasylishen, R. E. *J. Am. Chem. Soc.* **2006**, *128*, 7817.
(108) Feindel, K. W.; Ooms, K. J.; Wasylishen, R. E. *Phys. Chem. Chem. Phys.* **2007**, *9*, 1226.

ligand bonding (e.g., MO pairs involving occ MOs from 1 to 120 contribute to only 8.6% of the occ−vir paramagnetic contribution).

Let us consider a specific example to clarify the data in Table 5. The mixing of the occ MO 130 (HOMO −3) with virtual orbitals contributes −894.7 to the total paramagnetic shielding (σ_p) of −4272.2 ppm. Mixing of occ MO 130 with vir MO 138 (denoted as 130−138) accounts for −451.4 of the −894.7 ppm contributed by occ MO 130. The remaining contribution to shielding from occ MO 130 results from its mixing with many other virtual MOs, most notably vir MOs 139 and 144 (an extended data analysis including all of the occ−vir contributions can be found in Table S4).

The largest contributions to paramagnetic shielding arise from the mixing of a variety of occ MOs with vir MOs 138, 139, and 143 (Table 5). These virtual MOs are of high lead p orbital character, as demonstrated by the gross populations contributed by individual AOs (Table S5). MO 138 has relatively high lead $6p_y$ and slight 6s characters but also has significant contributions from carbon 2p orbitals on the neighboring aromatic rings. MO 139 and MO 143 are comprised of mixtures of large lead $6p_x$ and $6p_z$ AO contributions. The occupied MOs which mix with these three virtual MOs vary in their relative amounts of lead, sulfur, nitrogen, or carbon AO character. Large deshielding contributions involve occ MOs 130 to 133 (HOMO −3 to HOMO), and occ MOs 121, 122, 125, and 126. MO 133 corresponds to the stereochemically active lead lone pair, whereas MOs 130, 131, and 132 are largely localized on the sulfur atoms. MO 121 describes Pb−N bonding, MO 122 describes S−C σ bonding, MO 125 describes Pb−S bonding and S−C π bonding, and MO 126 describes S−C π bonding and some degree of localized nitrogen 2p character. Hence, the origin of the lead CS tensor is relatively complex and highly dependent upon the characteristics of the lead lone pair, 3p AOs localized on sulfur atoms, and variable types of σ and π bonding.

Understanding why certain MO pairs make large paramagnetic deshielding contributions can be accomplished through relatively simple visualization. MOs that contribute to shielding along the direction of a particular principal component must be relatively close in energy but also have the appropriate symmetries to interfere or overlap with one another when induced to mix by a magnetic field. This type of mixing can be visualized by rotating the appropriate MOs about the axes that define the principal components of the CS tensor. This concept has previously been demonstrated for several relatively simple systems.[52,105,106,108,109] We will use the arbitrary convention of right-handed 90 degree rotations of the virtual MOs about their gauge origin (i.e., contributing AOs are rotated in a right-handed fashion at the nuclear site). Rotations resulting in the constructive or destructive overlap of MO lobes generate deshielding and shielding contributions, respectively.[106] The simplest examples to consider are the 133−143 and 133−139 MO pairs

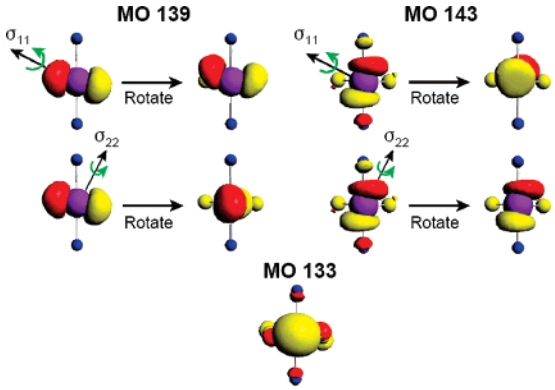

Figure 9. A representation of the rotation of vir MOs 139 and 143 of complex **2**. The axes of rotation correspond to the directions of σ_{11} and σ_{22} in the molecular frame. Only lead, sulfur, and nitrogen atoms are shown.

(Figure 9). The 133−143 MO pair makes significant deshielding contributions along σ_{11} and σ_{22}. A right-handed rotation of 143 about the σ_{11} axis results in a constructive overlap with 133, and similarly, the same rotation about σ_{22} leads to a constructive overlap, but to a lesser extent (and hence the smaller deshielding contribution). In the case of the 133−139 MO pair, rotation about σ_{11} does not generate any significant overlap, and the deshielding contribution is minimal. On the other hand, right-handed rotation about σ_{22} causes a large destructive overlap (i.e., lobes of opposite phases are overlapped), leading to a large shielding contribution. All of the other shielding and deshielding contributions can be rationalized and visualized in this manner, by simple rotations of the virtual orbitals.

Conclusions

We have studied the effects of varying the σ-electron donor ability of pyridine Lewis-base ligands on the coordination environment of lead(II) in bis-thiolate complexes. The reaction of $(2,6\text{-}Me_2C_6H_3S)_2Pb$ with a series of 4-substituted pyridines in toluene or dichloromethane led to the isolation of a series of 1:1 complexes. Solution ^1H, $^{13}C\{^1H\}$, and ^{207}Pb NMR spectra suggest that the coordination complexes are unstable in thf solutions and may only be studied in the solid state. X-ray crystallographic analysis shows compounds **3** and **4** to be dimeric, with a ψ-trigonal bipyramidal S_3N bonding environment for lead(II), whereas compound **5** is monomeric and exhibits a ψ-trigonal pyramidal S_2N bonding environment at lead(II). The structures may be rationalized using a simple bonding description, in which the axial lead−nitrogen and long intermolecular lead−sulfur dative bonding interactions occur via the empty 6p orbitals on lead(II). The lead−nitrogen bond distances were found to shorten with increasing σ-electron donor ability of the 4-substituted pyridine ligand. This affect was accompanied by a lengthening of the trans intermolecular lead−sulfur contact, which was absent for the strongest pyridine donor $pyNMe_2$ in compound **5**. This study demonstrates that novel bonding environments for lead(II) may be accessed through subtle alterations of Lewis-base donor ligands.

Lead CS tensor parameters have been measured from ^{207}Pb CP/CPMG solid-state NMR spectra for complexes **2**,

(109) Grutzner, J. B. In *Recent Advances in Organic NMR Spectroscopy*; Lambert, J. B., Rittner, R., Eds.; Norell Press: Landisville, 1987, p 17.

4, and **5**. The CP/CPMG sequence has been demonstrated to be much more efficient and accurate than MAS methods for the acquisition of the ^{207}Pb spectra of extremely broad, CSA-dominated powder patterns. Similar lead isotropic chemical shifts are observed within this series of compounds; however, CS tensor parameters are useful for differentiating the three types of lead coordination environments. DFT calculations that account for relativistic effects adequately reproduce the experimental CS tensor parameters and trends. Examination of the individual MOs generated by nonrelativistic calculations provides insight into the molecular origins of lead CS and evidence for the existence and position of the stereochemically active lone electron pair. Experimental measurement and theoretical calculations of lead CS tensor parameters are clearly useful for the elucidation of molecular and electronic structure, bonding, and symmetry.

Acknowledgment. G.G.B. thanks the Natural Sciences and Engineering Research Council (NSERC) of Canada, the New Brunswick Innovation Foundation (NBIF), and Mount Allison University for financial support. G.G.B. also thanks Mr. Dan Durant for assistance in collecting solution NMR data. R.W.S. thanks NSERC, the Canadian Foundation for Innovation (CFI), the Ontario Innovation Trust (OIT), and the Centre for Catalysis and Materials Research (CCMR) at the University of Windsor for funding. A.J.R. thanks the Ontario Ministry of Training, Colleges and Universities for an Ontario Graduate Scholarship. Mr. Cory M. Widdifield and Mr. Joel A. Tang are thanked for assistance with *ADF* calculations.

Supporting Information Available: X-ray crystallographic data for **3**−**5** in CIF format, powder X-ray diffraction patterns for compounds **2**, **4**, and **5**, additional ^{207}Pb and ^{13}C NMR data, and coordinates and energies for ab initio/DFT calculations where appropriate. This material is available free of charge via the Internet at http://pubs.acs.org. Crystallographic data for all of the structures in this article have been deposited with the Cambridge Crystallographic Data Centre, under CCDC 643476 (**3**), 643477 (**4**), and 643478 (**5**). Copies of this information may be obtained free of charge from The Director, CCDC, 12 Union Road, Cambridge CB2 1EZ, U.K. (fax, +44−1223-336033; e-mail, deposit@ccdc.cam.ac.uk; web, http://www.ccdc.cam.ac.uk).

IC700738W